ELSEVIER

PHYSICS LETTERS B

CrossMark

Study of the process $e^+e^- \to K_S^0 K_L^0$ in the center-of-mass energy range 1004–1060 MeV with the CMD-3 detector at the VEPP-2000 e^+e^- collider

E.A. Kozyrev [a,b,*], E.P. Solodov [a,b], A.N. Amirkhanov [a,b], A.V. Anisenkov [a,b],
V.M. Aulchenko [a,b], V.S. Banzarov [a], N.S. Bashtovoy [a], D.E. Berkaev [a,b], A.E. Bondar [a,b],
A.V. Bragin [a], S.I. Eidelman [a,b], D.A. Epifanov [a,b], L.B. Epshteyn [a,b,c], A.L. Erofeev [a,b],
G.V. Fedotovich [a,b], S.E. Gayazov [a,b], A.A. Grebenuk [a,b], S.S. Gribanov [a,b], D.N. Grigoriev [a,b,c],
F.V. Ignatov [a], V.L. Ivanov [a,b], S.V. Karpov [a], A.S. Kasaev [a], V.F. Kazanin [a,b], A.N. Kirpotin [a],
A.A. Korobov [a,b], O.A. Kovalenko [a,b], A.N. Kozyrev [a,b], I.A. Koop [a], P.P. Krokovny [a,b],
A.E. Kuzmenko [a,b], A.S. Kuzmin [a,b], I.B. Logashenko [a,b], P.A. Lukin [a,b], K.Yu. Mikhailov [a,b],
V.S. Okhapkin [a], A.V. Otboev [a], Yu.N. Pestov [a], A.S. Popov [a,b], G.P. Razuvaev [a,b], A.A. Ruban [a],
N.M. Ryskulov [a], A.E. Ryzhenenkov [a,b], A.I. Senchenko [a], V.E. Shebalin [a,b],
D.N. Shemyakin [a,b], B.A. Shwartz [a,b], D.B. Shwartz [a,b], A.L. Sibidanov [d], P.Yu. Shatunov [a],
Yu.M. Shatunov [a], V.M. Titov [a], A.A. Talyshev [a,b], A.I. Vorobiov [a], Yu.V. Yudin [a,b]

[a] *Budker Institute of Nuclear Physics, SB RAS, Novosibirsk, 630090, Russia*
[b] *Novosibirsk State University, Novosibirsk, 630090, Russia*
[c] *Novosibirsk State Technical University, Novosibirsk, 630092, Russia*
[d] *Department of Physics and Astronomy, P.O. Box 3055 Victoria, B.C., V8W 3P6, Canada*

ARTICLE INFO

ABSTRACT

The $e^+e^- \to K_S^0 K_L^0$ cross section has been measured in the center-of-mass energy range 1004–1060 MeV at 25 energy points using 6.1×10^5 events with $K_S^0 \to \pi^+\pi^-$ decay. The analysis is based on 5.9 pb^{-1} of an integrated luminosity collected with the CMD-3 detector at the VEPP-2000 e^+e^- collider. To obtain $\phi(1020)$ meson parameters the measured cross section is approximated according to the Vector Meson Dominance model as a sum of the ρ, ω, ϕ-like amplitudes and their excitations. This is the most precise measurement of the $e^+e^- \to K_S^0 K_L^0$ cross section with a 1.8% systematic uncertainty.

1. Introduction

Investigation of e^+e^- annihilation into hadrons at low energy provides unique information about interactions of light quarks. High-precision studies of various hadronic cross sections are of great interest in connection with the problem of the muon anomalous magnetic moment [1] and constitute the main goal of experiments with the CMD-3 and SND detectors at the upgraded VEPP-2000 collider [2,3].

In particular, $e^+e^- \to K_S^0 K_L^0$ is one of the processes with a rather large cross section in the center-of-mass energy range from 1 to 2 GeV. A precise measurement of this cross section, dominated by the contribution of the $\phi(1020)$ and $\phi(1680)$ resonances, is required to improve our knowledge of the hadronic contributions to $(g-2)_\mu$ and $\alpha(M_Z^2)$. Additional motivation for high-precision measurements of the $e^+e^- \to K_S^0 K_L^0$ and $e^+e^- \to K^+K^-$ cross sections around the ϕ meson peak comes from a significant deviation of the ratio of the coupling constants $\frac{g_{\phi \to K^+K^-}}{g_{\phi \to K_S K_L}}$ from theoretical predictions [4].

The most precise previous studies of the process have been performed at the CMD-2 [5], SND [6] and BaBar [7] detectors.

* Corresponding author.
 E-mail address: e.a.kozyrev@inp.nsk.su (E.A. Kozyrev).

In this paper we present results of the new measurement of the $e^+e^- \to K_S^0 K_L^0$ cross section based on a high-statistics data sample collected at 25 energy points in the center-of-mass energy (c.m.) $E_{c.m.}$ range 1004–1060 MeV with the CMD-3 detector.

2. CMD-3 detector and data set

The Cryogenic Magnetic Detector (CMD-3) described else-where [8] is installed in one of the two interaction regions of the VEPP-2000 e^+e^- collider [9]. The detector tracking system consists of the cylindrical drift chamber (DC) and double-layer cylindrical multiwire proportional Z-chamber, both installed inside a thin (0.085 X_0) superconducting solenoid with 1.3 T magnetic field. DC contains 1218 hexagonal cells and provides a measurement of charged particle momentum and of the polar (θ) and azimuthal (ϕ) angles. An amplitude information from the DC wires is used to measure the ionization losses dE/dx of charged particles with $\sigma_{dE/dx} \approx$ 11–14% accuracy for minimum ionization particles (m.i.p.). A barrel electromagnetic calorimeter placed outside the solenoid consists of two subsystems: an inner liquid xenon (LXe) calorimeter (5.4 X_0 thick) surrounded by a scintillation CsI crystal calorimeter (8.1 X_0 thick) [10]. BGO crystals with 13.4 X_0 are used as an endcap calorimeter. The detector has two triggers: neutral and charged. A signal for neutral one is generated by the information from calorimeters, while the charged trigger comes from the tracking system. The return yoke of the detector is surrounded by scintillation counters which veto cosmic events.

To obtain a detection efficiency, Monte Carlo (MC) simulation of the detector based on the GEANT4 [11] package has been developed. Simulated events are subject to the same reconstruction and selection procedures as the data. MC simulation includes photon jet radiation by initial electrons calculated according to Refs. [12, 13]. Background was estimated using a multihadronic Monte Carlo generator [14] based on experimental data for all measured processes in the energy range up to 2 GeV.

The analysis uses 5.9 pb^{-1} of an integrated luminosity collected in two scans of the $\phi(1020)$ resonance region at 25 energy points in the $E_{c.m.}$ = 1004–1060 MeV range. The beam energy E_{beam} has been monitored by using the Back-Scattering-Laser-Light system [15,16] which determines $E_{c.m.}$ at each energy point with about 0.06 MeV accuracy.

3. Event selection

Signal identification is based on detection of two pions from the $K_S^0 \to \pi^+\pi^-$ decay. For each pair of oppositely charged tracks a constrained fit to a common vertex is performed to determine track parameters. Assuming tracks to be pions, the pair with the best χ^2 from the vertex fit and with the invariant mass in the range 420–580 MeV/c^2 is selected as a K_S^0 candidate. The following requirements are applied to events with a found K_S^0 candidate:

- The longitudinal distance and the transverse coordinate of the vertex should have $|Z_{K_S^0}| <$ 10 cm and $|\rho_{K_S^0}| <$ 6 cm, respectively;
- Pions from K_S^0 decay are required to have polar angles $1 < \theta_{\pi^+,\pi^-} < \pi - 1$ radians;
- Each track has momentum 130 MeV/c $< P_{\pi^\pm} <$ 320 MeV/c corresponding to the kinematically allowed region for pions from the K_S^0 decay and its ionization losses in DC are within three standard deviations from the average value, expected for pions. The last requirement rejects charged kaons and back-
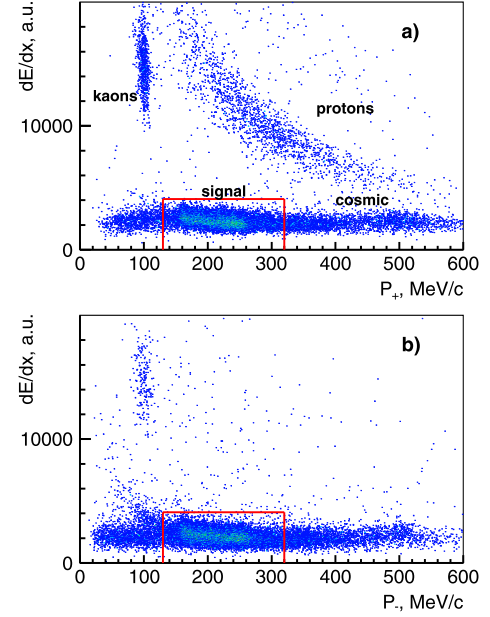

Fig. 1. Ionization losses vs momentum for positive (a) and negative (b) tracks for data at E_{beam} = 505 MeV. The lines show selections of pions from the K_S^0 decay.
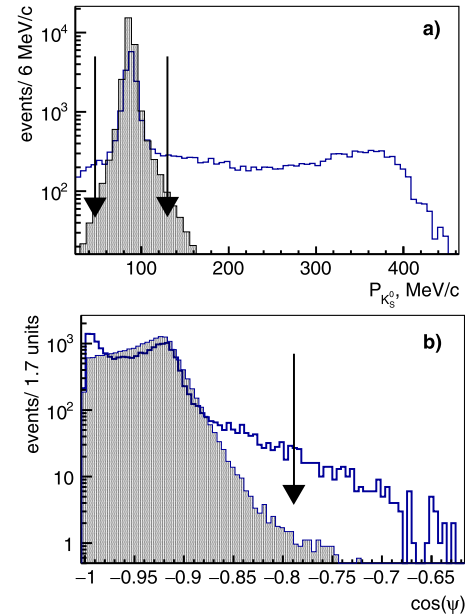

Fig. 2. Total momentum $P_{K_S^0}$ (a) and cosine of the angle ψ between the two charged pions (b) for the K_S^0 candidates after preliminary selection for data (open histogram) and MC simulation (shaded histogram) at E_{beam} = 505 MeV. The arrows show additional selection requirements.

ground protons, as shown in Fig. 1 for positive (a) and negative (b) tracks, respectively, at E_{beam} = 505 MeV;
- The momentum of the K_S^0 candidate, $P_{K_S^0} = |\vec{P}_{\pi^+} + \vec{P}_{\pi^-}|$, is required to be not larger than five standard deviations from the nominal momentum $P_{K_S^0} = \sqrt{E_{c.m.}^2/4 - m_{K_S^0}^2}$ at each energy, as shown by the arrows in Fig. 2(a);
- The cosine of the angle ψ between the tracks should be smaller than the cosine of the minimal angle between two pions originating from the two-body decay of the K_S^0 meson, shifted by five standard deviations, as shown by the arrow in Fig. 2(b).
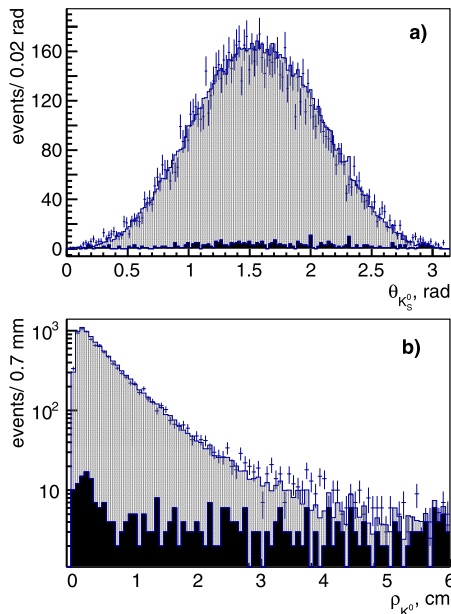
Fig. 3. Reconstructed polar angle of the K_S^0 meson (a) and the transverse distance of the K_S^0 decay vertex from the beam (b) at $E_{\text{beam}} = 505$ MeV for data (points) and signal simulation (shaded histogram). The dark shaded histograms represent the estimated contribution from the background processes.

The reconstructed polar angle of the K_S^0 meson and the transverse distance of the K_S^0 decay vertex from the e^+e^- interaction point are shown in Fig. 3 after above selections for data (points) and MC-simulation (shaded histogram). The dark shaded histograms show a sum of the background contributions from the MC-simulated hadronic processes (predominantly $e^+e^- \to \pi^+\pi^-2\pi^0$) and a contribution from cosmic muons estimated using events from the $|Z_{K_S^0}|$ sideband ($10 < |Z_{K_S^0}| < 15$ cm).

We determine the number of signal events for data and simulation from a binned maximum likelihood fit of two-pion invariant mass shown in Fig. 4. The signal shape is described by a sum of four Gaussian functions with parameters fixed from the simulation and with additional Gaussian smearing to account for the difference in data-MC detector responses. The background in data, described by a second-order polynomial function, constitutes about 30% outside the ϕ meson peak and 0.5% under it. By toy MC experiments with fixed signal and background profiles as well as by varying the background shape and approximation range used we estimate an uncertainty on the number of extracted signal events as less than 1.1%. The number of obtained signal events, N_{exp}, for each energy is listed in Table 3.

4. Cross section of $e^+e^- \to K_S^0 K_L^0$

The Born cross section of the process $e^+e^- \to K_S^0 K_L^0$ is calculated at each energy from the expression:

$$\sigma^{\text{Born}} = \frac{N_{\text{exp}}}{\epsilon_{\text{reg}}\epsilon_{\text{trig}}L(1+\delta^{\text{rad.}})}(1+\delta^{\text{en.spr.}}), \qquad (1)$$

where ϵ_{reg} is a detection efficiency, ϵ_{trig} is a trigger efficiency, L is an integrated luminosity, $1+\delta^{\text{rad.}}$ is a radiative correction, and $1+\delta^{\text{en.spr.}}$ represents a correction due to the spread of the collision energy.

The detection efficiency ϵ_{reg} is obtained by dividing the number of MC simulated events after reconstruction and selection described above by the total number of generated $K_S^0 K_L^0$ pairs taking into account the branching fraction $B_{K_S^0 \to \pi^+\pi^-} = (69.20 \pm$
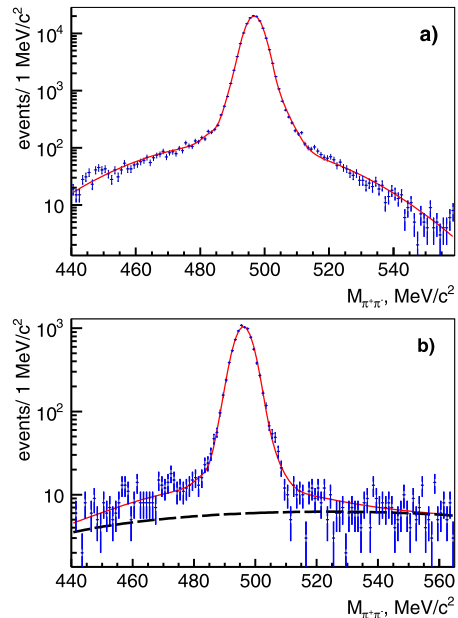

Fig. 4. Approximation of the invariant mass of two pions at $E_{\text{beam}} = 505$ MeV for simulation (a) and data (b). The solid line corresponds to the signal, the long-dotted line to the background.
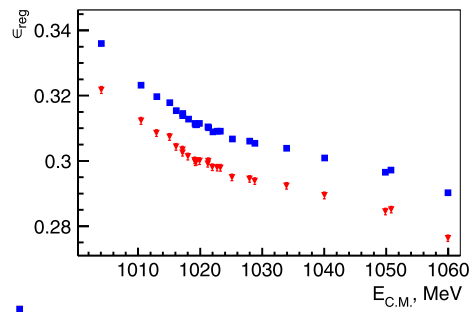

Fig. 5. Detection efficiency of the $K_S^0 K_L^0$ pairs vs energy from simulation (triangles). The geometrical efficiency is shown by squares (see text).

0.05)% [17]. Fig. 5 shows the obtained detection efficiency (triangles) vs c.m. energy in comparison with the expected geometrical efficiency (squares). The geometrical efficiency is calculated as the probability of pions to be in the polar angle range $1 < \theta_{\pi^+,\pi^-} < \pi - 1$ radians at the generator level.

The trigger efficiency is studied using responses of two independent triggers, charged and neutral, for selected signal events, and is found to be close to unity, $\epsilon_{\text{trig}} = 0.998 \pm 0.001$.

The integrated luminosity L is determined using events of the processes $e^+e^- \to e^+e^-$ (Bhabha events) with about 1% [18] systematic accuracy.

The initial-state radiative correction $1 + \delta^{\text{rad.}}$, shown by squares in Fig. 6, is calculated using the structure function method with an accuracy better than 0.1% [19].

The spread of collision energy is about 350 keV, that is significant in comparison with the ϕ meson width, and we introduce the correction of the cross section, shown by points in Fig. 6, which has a maximum value of 1.028 ± 0.004 at the peak of the ϕ resonance.

The resulting cross section is listed in Table 3 for each energy and shown in Fig. 8. The presented errors are statistical only and include fluctuations of signal and Bhabha events as well as the error $\delta E_{\text{c.m.}}$ due to the statistical uncertainty of the c.m. energy measurement. The last part was calculated as $|\frac{\partial\sigma^{\text{Born}}}{\partial E_{\text{c.m.}}}| \times \delta E_{\text{c.m.}}$.
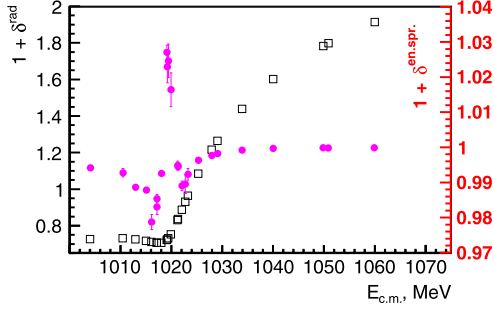
Fig. 6. Radiative corrections $1 + \delta^{\text{rad.}}$ (squares, left scale) and corrections $1 + \delta^{\text{en.spr.}}$ for the spread of collision energy (points, right scale).
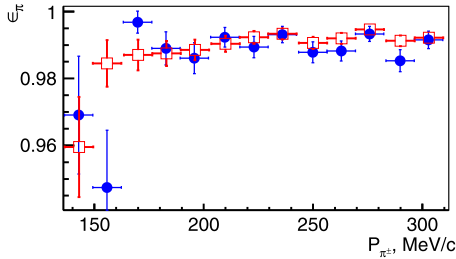

Fig. 7. Pion detection efficiency in DC vs momentum for data (circles) and simulation (squares).

5. Systematic uncertainties

MC simulation may not exactly reproduce all detector responses, so an additional study was performed to obtain corrections for data-MC difference in the detection efficiency.

The data-MC difference in the charged pion detection by DC is studied using the process $e^+e^- \to \phi \to \pi^+\pi^-\pi^0$. Three-pion events can be fully reconstructed from one detected charged track and two detected photons from the π^0 decay, and a probability to detect another charged track can be determined. For the polar angle requirement $1 < \theta_{\pi^+,\pi^-} < \pi - 1$ radians, the average detection inefficiency is about 1% per track for high momentum, and decreases with pion momentum, as shown in Fig. 7. The rise of efficiency vs momentum is explained by the decreasing number of pions that decayed or interacted in DC. Good data-MC agreement is observed for charged pion detection, so no efficiency correction is introduced and the uncertainty in the detection is estimated as 0.5%.

DC calibration is checked using signals of the Bhabha events [18] in the DC and Z-chamber, and for pions from the K_S^0 decay the uncertainty due to the polar angle selection in the range of polar angles chosen is estimated as 0.4%.

By variation of corresponding selection criteria we estimate the uncertainty due to the data-MC difference in the angular and momentum resolutions as 0.5%, while other selection criteria contribute another 0.6%.

The total uncertainty of the detection efficiency is calculated as a quadratic sum of uncertainties from the different sources and is estimated to be 1.0%.

The systematic uncertainties of the $e^+e^- \to K_S^0 K_L^0$ cross section discussed above are summarized in Table 1 giving 1.8% in total.

6. Fitting of the $e^+e^- \to K_S^0 K_L^0$ cross section

To obtain $\phi(1020)$ parameters we approximate the energy dependence of the cross section according to the vector meson dom-

Table 1
Summary of systematic uncertainties in the $e^+e^- \to K_S^0 K_L^0$ cross section measurement.

Source	Uncertainty, %
Signal extraction by fit	1.1
Detection efficiency	1.0
Radiative correction	0.1
Energy spread correction	0.3
Trigger efficiency	0.1
Luminosity	1.0
Total	1.8

inance (VMD) model as a sum of the ρ, ω, ϕ-like amplitudes [20]:

$$\sigma_{e^+e^- \to K_S^0 K_L^0}(s) = \frac{8\pi\alpha}{3s^{5/2}} p_{K^0}^3 \left| \frac{g_{\rho\gamma} g_{\rho KK}}{D_\rho(s)} + \frac{g_{\omega\gamma} g_{\omega KK}}{D_\omega(s)} \right.$$
$$\left. + \frac{g_{\phi\gamma} g_{\phi KK}}{D_\phi(s)} + A_{\rho',\omega',\phi'} \right|^2, \tag{2}$$

where $s = E_{\text{c.m.}}^2$, p_{K^0} is a neutral kaon momentum, $D_V(s) = m_V^2 - s - i\sqrt{s}\Gamma_V(s)$, m_V, and Γ_V are mass and width of the major intermediate resonances: $V = \rho(770)$, $\omega(782)$, $\phi(1020)$. The energy dependence of the decay width is expressed via a sum of partial widths multiplied by a factor of phase space energy dependence $P_{V \to f}(s)$ of each decay mode as:

$$\Gamma_V(s) = \Gamma_V \sum_{V \to f} B_{V \to f} \frac{P_{V \to f}(s)}{P_{V \to f}(m_V^2)}.$$

The coupling constants of the intermediate vector meson V with initial and final states can be presented as:

$$|g_{V\gamma}| = \sqrt{\frac{3m_V^3 \Gamma_{Vee}}{4\pi\alpha}}; \quad |g_{VKK}| = \sqrt{\frac{6\pi m_V^2 \Gamma_V B_{VKK}}{p_{K^0}^3(m_V)}},$$

where Γ_{Vee} and B_{VKK} are electronic width and branching fraction of the V meson decay to a pair of kaons.

In our approximation we use the world-average values of mass, total width and electronic width of the $\rho(770)$ and $\omega(782)$: $\Gamma_{\rho \to ee} = 7.04 \pm 0.06$ keV, $\Gamma_{\omega \to ee} = 0.60 \pm 0.02$ keV [17]. The branching fractions of the $\rho(770)$ and $\omega(782)$ to a kaon pair are unknown, and we use the relation $g_{\omega K_S^0 K_L^0} = -g_{\rho K_S^0 K_L^0} = -g_{\phi K_S^0 K_L^0}/\sqrt{2}$, based on the quark model with "ideal" mixing and exact SU(3) symmetry of u-, d-, s-quarks [20].

The amplitude $A_{\rho',\omega',\phi'}$ denotes a contribution of excited $\rho(1450)$, $\omega(1420)$ and $\phi(1680)$ vector meson states in the $\phi(1020)$ mass region. Using BaBar [7] data above 1.06 GeV for the process $e^+e^- \to K_S^0 K_L^0$ we found a relatively small contribution of these states in the studied energy range in comparison with nonresonant ρ and ω contributions.

We perform a fit to the $e^+e^- \to K_S^0 K_L^0$ cross section with floating m_ϕ, Γ_ϕ, and $\Gamma_{\phi \to ee} \times B_{\phi \to K_S^0 K_L^0}$ (or alternatively $B_{\phi \to ee} \times B_{\phi \to K_S^0 K_L^0}$) parameters: the fit yields $\chi^2/ndf = 20/22$ ($P(\chi^2) = 58\%$). The contributions of the ρ and ω intermediate states are non-negligible and we performed a fit where we introduce an additional floating parameter $g_{\rho,\omega}$, which is a multiplicative factor for both $g_{\omega K_S^0 K_L^0}$ and $g_{\rho K_S^0 K_L^0}$ coupling constants in Eq. (2). The fit yields $\chi^2/ndf = 15/21$ ($P(\chi^2) = 82\%$) with $g_{\rho,\omega} = 0.80 \pm 0.09$. This is the first quantitative estimate of the ρ and ω amplitude contributions in the ϕ meson region. The obtained parameters of the ϕ meson in comparison with the values of other measurements are presented in Table 2 and the fit result is shown in Fig. 8(a). Fig. 8(b) shows the relative difference between the obtained data

Table 2
The results of the approximation procedure in comparison with previous experiments.

Parameter	CMD-3	Other measurements
m_ϕ, MeV	$1019.457 \pm 0.006 \pm 0.060 \pm 0.010$	1019.461 ± 0.019 (PDG2014)
Γ_ϕ, MeV	$4.240 \pm 0.012 \pm 0.005 \pm 0.010$	4.266 ± 0.031 (PDG2014)
$\Gamma_{\phi \to ee} B_{\phi \to K_S^0 K_L^0}$, keV	$0.428 \pm 0.001 \pm 0.008 \pm 0.005$	0.4200 ± 0.0127 (BaBar)
$B_{\phi \to ee} B_{\phi \to K_S^0 K_L^0}$, 10^{-5}	$10.078 \pm 0.025 \pm 0.188 \pm 0.118$	10.06 ± 0.16 (PDG2014)

Table 3
The c.m. energy $E_{c.m.}$, number of selected signal events N, detection efficiency ϵ_{MC}, radiative-correction factor $1 + \delta_{rad.}$, integrated luminosity L, and Born cross section σ of the process $e^+ e^- \to K_S^0 K_L^0$. Statistical errors only are shown.

|	$E_{c.m.}$, MeV	N events	ϵ_{MC}	$1 + \delta_{rad.}$	$1 + \delta_{en.spr.}$	L, nb^{-1}	σ, nb
1	1004.066 ± 0.008	315 ± 19	0.321	0.72	0.994	195.35 ± 0.67	6.87 ± 0.42
2	1010.466 ± 0.010	9083 ± 100	0.312	0.73	0.992	936.05 ± 1.44	42.16 ± 0.47
3	1012.955 ± 0.007	10639 ± 108	0.308	0.72	0.988	485.35 ± 1.04	96.74 ± 1.00
4	1015.068 ± 0.012	2347 ± 50	0.307	0.71	0.987	47.91 ± 0.33	219.53 ± 5.02
5	1016.105 ± 0.010	15574 ± 130	0.304	0.71	0.978	192.11 ± 0.66	366.33 ± 3.33
6	1017.155 ± 0.012	65612 ± 264	0.303	0.70	0.983	478.99 ± 1.04	628.15 ± 2.95
7	1017.156 ± 0.013	5525 ± 77	0.302	0.70	0.985	40.76 ± 0.3	624.76 ± 9.89
8	1018.046 ± 0.021	102233 ± 334	0.301	0.70	0.992	478.34 ± 1.04	996.62 ± 4.28
9	1019.118 ± 0.016	98014 ± 326	0.3	0.72	1.028	328.62 ± 0.86	1413.65 ± 6.02
10	1019.214 ± 0.019	16059 ± 132	0.299	0.72	1.022	52.75 ± 0.34	1433.05 ± 15.03
11	1019.421 ± 0.028	11066 ± 110	0.299	0.73	1.024	36.04 ± 0.28	1434.84 ± 18.40
12	1019.902 ± 0.012	140758 ± 386	0.299	0.75	1.016	472.34 ± 1.04	1341.91 ± 4.74
13	1021.222 ± 0.021	47552 ± 225	0.299	0.83	0.994	228.34 ± 0.72	833.20 ± 4.89
14	1021.309 ± 0.009	9545 ± 102	0.299	0.83	0.994	46.85 ± 0.33	807.54 ± 10.36
15	1022.078 ± 0.021	31323 ± 183	0.297	0.88	0.989	201.61 ± 0.68	582.93 ± 4.03
16	1022.744 ± 0.019	14517 ± 126	0.297	0.93	0.989	116.71 ± 0.52	443.71 ± 4.38
17	1023.264 ± 0.025	6876 ± 86	0.297	0.96	0.992	62.91 ± 0.38	377.77 ± 5.31
18	1025.320 ± 0.031	2319 ± 51	0.294	1.08	0.996	36.32 ± 0.28	199.26 ± 4.97
19	1027.956 ± 0.015	8150 ± 94	0.294	1.21	0.997	195.83 ± 0.67	115.93 ± 1.70
20	1029.090 ± 0.014	1911 ± 45	0.293	1.26	0.998	52.94 ± 0.35	96.96 ± 3.00
21	1033.907 ± 0.011	3704 ± 64	0.292	1.43	0.999	175.55 ± 0.64	50.12 ± 1.26
22	1040.028 ± 0.035	2839 ± 56	0.289	1.6	1	195.91 ± 0.68	31.27 ± 1.01
23	1049.864 ± 0.011	4291 ± 70	0.284	1.78	1	499.59 ± 1.09	16.93 ± 0.50
24	1050.862 ± 0.031	1310 ± 39	0.285	1.79	1	146.31 ± 0.59	17.47 ± 0.94
25	1059.947 ± 0.015	1271 ± 38	0.276	1.91	1	198.86 ± 0.69	12.09 ± 0.71
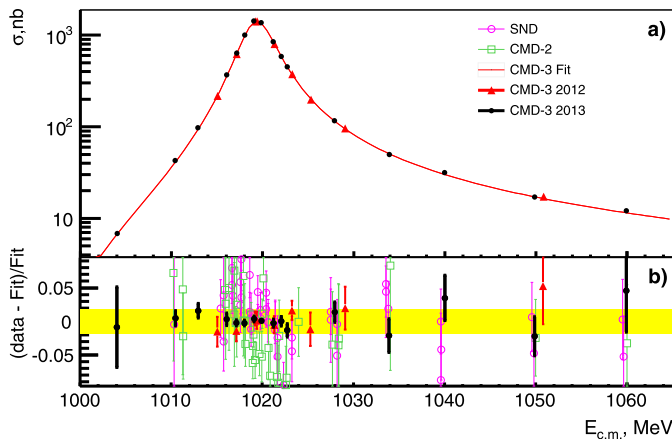
Fig. 8. (a) Measured $e^+ e^- \to K_S^0 K_L^0$ cross section in comparison with previous experiments. The dots are experimental data, the curve is the fit described in the text. (b) Relative difference between the data and fit. Comparison with other experimental data is shown. Statistical uncertainties only are included for data. The width of the band shows the systematic uncertainties in our experiment.

and the fit curve. Only statistical uncertainties are shown. The width of the band shows the systematic uncertainty in our measurement. A slope of the CMD-2 points [5] can be explained by an
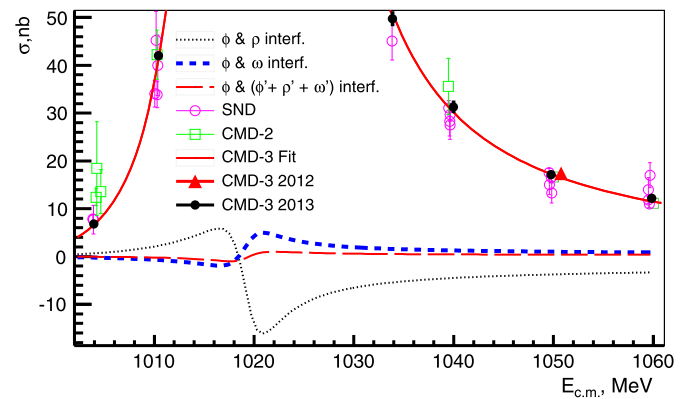

Fig. 9. Contributions of lower- and higher-mass resonances to the fit of the $e^+ e^- \to K_S^0 K_L^0$ cross section in the studied energy range.

about 80 keV difference between the used values of c.m. energy in the previous work and this experiment, that is within declared systematic uncertainties of the energy measurements.

The contributions of the ρ and ω intermediate states are demonstrated in Fig. 9 by the dotted lines, while the long-dashed line shows a contribution from higher excitations. The first uncertainties presented in Table 2 are statistical, and the second are the
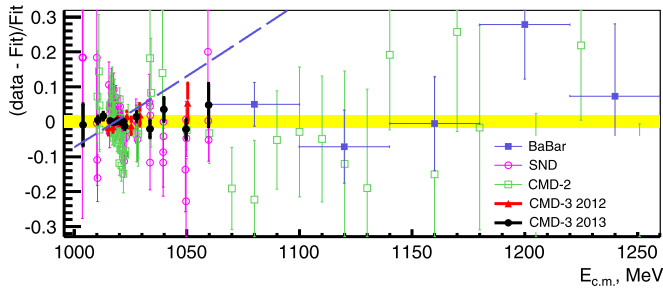
Fig. 10. Relative difference between the data and fit for the $E_{c.m.} = 1.00–1.25$ GeV range. The dashed line is the contribution of the ϕ meson amplitude only.

$$m_\phi = 1019.457 \pm 0.061 \text{ MeV}/c^2$$

$$\Gamma_\phi = 4.240 \pm 0.017 \text{ MeV}$$

$$\Gamma_{\phi \to ee} B_{\phi \to K_S^0 K_L^0} = 0.428 \pm 0.009 \text{ keV}.$$

The obtained parameters are in good agreement with previous experiments. The values of Γ_ϕ and $\Gamma_{\phi \to ee} B_{\phi \to K_S^0 K_L^0}$ are the most precise among all existing measurements. High precision in the cross section measurement allows the first quantitative estimate of the contributions from ρ and ω mesons to the studied c.m. region.

Acknowledgements

References

[1] T. Blum, et al., arXiv:1311.2198.
[2] M.N. Achasov, et al., Phys. Rev. D 91 (2015) 092010.
[3] D.N. Shemyakin, et al., Phys. Lett. B 756 (2016) 153.
[4] A. Bramon, et al., Phys. Lett. B 486 (2000) 406.
[5] R.R. Akhmetshin, et al., CMD-2 Collaboration, Phys. Lett. B 695 (2011) 412.
[6] M.N. Achasov, et al., SND Collaboration, Phys. Rev. D 63 (2001) 072002.
[7] J.P. Lees, et al., BaBar Collaboration, Phys. Rev. D 89 (2014) 092002.
[8] B.I. Khazin, et al., Nucl. Phys. B, Proc. Suppl. 376 (2008) 181.
[9] Yu.M. Shatunov, et al., in: Proceedings of the 7th European Particle Accelerator Conference, Vienna, 2000, p. 439.
[10] V.M. Aulchenko, et al., J. Instrum. 10 (2015) P10006.
[11] S. Agostinelli, et al., GEANT4 Collaboration, Nucl. Instrum. Methods Phys. Res., Sect. A, Accel. Spectrom. Detect. Assoc. Equip. 506 (2003) 250.
[12] A.B. Arbuzov, et al., Eur. Phys. J. C 46 (2006) 689.
[13] S. Actis, et al., Working group for radiative corrections and Monte Carlo generators at low energies, Eur. Phys. J. C 66 (2010) 585.
[14] H. Czyż, et al., arXiv:1312.0454.
[15] E.V. Abakumova, et al., Nucl. Instrum. Methods Phys. Res., Sect. A 744 (2014) 35.
[16] E.V. Abakumova, et al., J. Instrum. 10 (2015) T09001.
[17] K.A. Olive, et al., Particle Data Group, Chin. Phys. C 38 (2014) 090001.
[18] G.V. Fedotovich, et al., Phys. At. Nucl. 78 (2015) 591.
[19] E.A. Kuraev, V.S. Fadin, Sov. J. Nucl. Phys. 41 (1985) 466.
[20] C. Bruch, A. Khodjamirian, J. Kühn, Eur. Phys. J. C 39 (2005) 41.

systematic uncertainties. Two effects were taken into account in the estimation of the latter: the accuracy of the measurement of the c.m.s. energy $E_{c.m.}$ of 60 keV and the systematic uncertainty of the cross section measurement of 1.8% (Table 1). To study model dependence of the results, several additional fits are performed. Other fits use Eq. (2) without the $A_{\phi',\rho',\omega'}$ amplitude and introduce an additional floating phase of the ϕ meson amplitude or the both ρ and ω amplitudes. The variations in the ϕ meson parameters are used as an estimate of the model-dependent uncertainty presented as a third uncertainty in Table 2. The obtained values agree with results of other measurements and some are more precise.

Fig. 10 shows available experimental data up to $E_{c.m.} = 1250$ MeV and demonstrates that the obtained fit parameters do not contradict other measurements at higher $E_{c.m.}$ values. The dashed line shows the contribution of the ϕ meson only, when the amplitudes from the $\rho(770)$ and $\omega(782)$ are excluded demonstrating that the destructive interference with these states dominates in the shown energy region.

7. Conclusion

Using the $K_S^0 \to \pi^+ \pi^-$ decay we observe 6.1×10^5 events of the process $e^+ e^- \to K_S^0 K_L^0$ in the 1004–1060 MeV c.m. energy range, and measure the cross section with a 1.8% systematic uncertainty. The following values of the ϕ meson parameters have been obtained: